Thermochromoluminescent Mn2+-doped oxides as thermal sensor for selective laser sintering

François Rouzé L'alzit, Tiphaine Bazin, Angeline Poulon-Quintin, Eric Champion, Caroline Bertrand, Thierry Cardinal, Aline Rougier, Issam Mjejri, Veronique Jubera, Manuel Gaudon

THERMOCHROMOLUMINESCENT Mn^{2+}-DOPED OXIDES AS THERMAL SENSOR FOR SELECTIVE LASER SINTERING

François Rouzé l'Alzit[1], Tiphaine Bazin,[1,2] Angéline Poulon-Quintin,[1] Eric Champion,[2] Caroline Bertrand,[1] Thierry Cardinal,[1] Aline Rougier,[1] Issam Mjejri,[1] Véronique Jubera,[1] Manuel Gaudon[1]

[1] CNRS, Univ. Bordeaux, Bordeaux INP, Institut de Chimie de la Matière Condensée de Bordeaux, UMR 5026, Pessac, France

[2] Université de Limoges, CNRS, Institut de Recherche sur les Céramiques, UMR 7315, Limoges, France
*corresponding author: manuel.gaudon@icmcb.cnrs.fr / 0033 5 40 00 66 85

Abstract

Mn^{2+}-doped $Zn_3(PO_4)_2$ and Mn^{2+}-doped $ZnAl_{2.2}O_{4+\delta}$ compounds were prepared from solid state route and Pechini process, respectively. The luminescent properties evolution of both as-prepared powder compounds versus the annealing temperature (for 10 min annealing treatments) was studied, in the range 500-1400°C. In parallel, Doctor Blade was used to prepare few micron-thick films for laser irradiation with the 1μm wavelength laser of our SLS process (Selective Laser Sintering process). The ultra-rapid heating produces by laser irradiation induces on the films very different optical properties evolution in comparison to what was observed for the powder samples annealed into furnaces for the Mn-doped zinc phosphate. On the opposite, for the spinel compound, whatever the heating process (laser on film or furnace for powder samples), the modification of the luminescence properties is directly linked in a same way to the maximum temperature gained during the thermal history. The idea is to use thermal sensor to extract the temperature map of a film while it is subjected to laser irradiation as during SLS process. The study shows that thermal sensors must rely on mechanisms which remain effective even for ultra-rapid heating: a cationic redistribution versus temperature as occurring into spinel matrix is one solution proposed. But changes in the chromaticity resulting from phase transition between different allotropic forms as occurring into the zinc phosphate compound cannot be directly exploited.

1. Introduction

The development of 3D-printing (or additive manufacturing) has encouraged the manufacture of small-scale parts while reducing production time of limited or custom series since certain steps such as mould making are no longer useful [1]. Coupling of the shaping technique with numerical modelling and simulation tools allows the production of complex shapes, whether geometrically or hierarchically: objects with cavities, inclusions or alveolar structures can be easily printed. The manufacturing is therefore called “additive process” in the sense that the shaping of a three-dimensional piece results from the addition of matter thanks to powder sintering, layer by layer. Among, additive synthesis processes, the selective laser sintering process involves the sintering of powder particles (metal, ceramics, polymer, glass) using a laser heating. Each powder layer undergoes a two-dimensional structuring before being covered with a new layer. Most of the commercially available SLS machines are equipped with Nd:YAG laser or ytterbium doped laser [2-6]. The interaction of the laser beam with the powder produces a local heating at a temperature close or higher than the powder melting point; this causes the particles to partially fuse, allowing the powder to be consolidated thanks to sintering phenomenon.

On one hand, the transferred energy depends on both the thermal conductivity and melting point of the powder and its optical absorption at the wavelength of laser radiation. If the applied energy is too weak, the consolidation between the particles themselves and the different layers will be insufficient leading to porous and brittle objects [7]. However, too much energy causes the total melting of particles that rearrange themselves to minimize their surface energy forming solidified droplets: this phenomenon being sometimes named “balling effect” [8, 9] and or with modification of the composition and porosity formation. Delamination of the sintered layers and the formation of cracks can also be observed due to high cooling rates and so, residual stresses [7]. Each compound will have to be studied to determine the optimal Laser regime to apply, directly linked to the reached local temperature distribution obtained. Besides, the SLS manufacturing technique, involving compulsory and significant thermal variations that cause stresses, is therefore subject to many

limitations. Especially, for ceramic materials, the rapid heating of the laser-irradiated area at very high temperatures (ceramics characterized by typically very high melting points) combined with low thermal conductivity (ceramic and thermal insulating materials) result in very high local temperature gradient within the ceramic [10]. Besides, ceramics are known as brittle materials, not elastic materials. The laser process can result in detrimental mechanical constraints if process parameters are not well selected. Hence, selective laser sintering has been extensively studied on polymers (PVC, , etc.) or metallic materials [4-6]. In the case of ceramics, although the laser beam can induce a temperature high enough to ensure the densification of ceramics due to advanced sintering, it is difficult to achieve the local densification of ceramic powders [11-12], and ceramics are much more prone to constrains induced by the temperature gradient mentioned above causing large cracks formation. Nowadays, the use of an organic binder to perform “indirect selective laser sintering” is largely predominant in literature for ceramic preparation resulting from additive manufacturing [13-16]. Furthermore, as another drawback for the direct SLS process, it has been observed that samples irradiated with the same laser energy density but from distinct laser power / lasing writing speed pairs have a different microstructure affecting the density and final mechanical properties of the sample [17-19]. So, the local temperature control is complex for ceramic powder. The energy applied to a line on the powder bed is directly related to the power composition, powder bed density and powder particle size distribution, and to the scanning speed of the laser such as the applied linear energy is proportional to the power of the laser and inversely proportional to the scanning speed. But different temperature gradients, leading to various widths for the irradiated zone line, the occurrence or not of the balling effect, are produced from same laser energy depending on the laser power / laser speed couple [20-22]. *A priori*, the thermal profiles according to the width of the lased line respond to characteristic profiles of the Gaussian beams, by means both the Gaussian dispersion of laser radiation intensities according to this axis, but also the thermal conductivity profiles within the material. But, as far as we know, the thermal profile of the lased track produced on the ceramic powder layers during the SLS process is not experimentally measured and clearly reported in

literature. Nonetheless, the accurate control of the temperature gradients is the key parameter to achieve the final 3D piece with optimized microstructure: surface roughness, density, absence of defects (cracks, pores), high relative density and so good mechanical properties as shown in the rare reports of a successful use of direct SLS for small ceramic pieces production [2].

On the other hand, additive manufacturing of phosphate materials and especially bio-phosphate materials is of great interest, and at the same time, Mn^{2+}-doped $Zn_3(PO_4)_2$ phosphate exhibits a rich thermal history with numerous events [23]. For such compound, various allotropic forms can be stabilized with irreversible transitions for a 600°C up to 1000°C temperature range. The Mn^{2+} transition metal can occupy distorted tetrahedral or octahedral sites depending on the low or high temperature form. Hence, versus the thermal history of the samples, different types of emission spectra can be obtained. By increasing the annealing temperature, the green emission associated with Mn^{2+} in a tetrahedral environment progressively disappears in favour of the red one that corresponds to Mn^{2+} stabilized in five- and six-fold coordination sites. The chromaticity of Mn^{2+}-doped $Zn_3(PO_4)_2$ strongly changes in the 600°C - 1000°C range, and one can consider this phosphate as an interesting thermal sensor. The additive manufacturing of aluminium based oxide is also extensively proposed in literature. Mn^{2+}-doped $ZnAl_{2.2}O_{4+\delta}$ phosphors get in the same way a large change of emission spectra after annealing treatment from 600 °C up to 1400 °C [24]. As the annealing temperature increases, the global inversion rate, which characterizes the cation distribution in both A and B sites of the spinel structure, decreases leading to a more direct matrix. So, the red luminescence related to the presence of Mn^{2+} in octahedral sites fades away to be replaced by a new green emission due to Mn^{2+} ions located in tetrahedral sites within the spinel structure. Such properties lead to consider the Mn-doped zinc-aluminium spinel as a potential candidate for developing stable and highly sensitive thermal sensors.

In this article, we propose to use the two thermal sensors Mn^{2+}-doped $Zn_3(PO_4)_2$ and Mn^{2+}-doped $ZnAl_{2.2}O_{4+\delta}$ as material for SLS process temperature probe. Laser tracks are realized on 2D films of these two ceramic compositions previously prepared by Dr Blade process. Then micro-

luminescence using confocal microscope is utilized to analyse post mortem the temperature gradient reached during laser process. The study aims to show that such thermochromoluminescent materials, able to change their emission spectra with temperature, could be the solution to optimize the control of the laser-matter interaction during the SLS process of metallic or ceramic materials.

2. Materials and methods

2.1. Samples preparation

The Mn^{2+}-doped $Zn_3(PO_4)_2$ compound was synthetized by aqueous co-precipitation method: stoichiometric amounts of $ZnCl_2$,$6H_2O$ and $MnCl_2$,$6H_2O$ were previously dissolved in aqueous medium and added dropwise in an equimolar solution of $(NH_4)_2HPO_4$. The reaction was performed under vigorous stirring at room temperature with three hours of ripening. Then, the as-prepared precipitate was allowed to dry at ambient temperature.

The $Zn_{0.95}Mn_{0.05}Al_{2.2}O_{4+\delta}$ sample was synthetized by the Pechini route. Stoichiometric amounts of zinc nitrate hexahydrate, aluminium nitrate nonahydrate and manganese nitrate hydrate were dissolved in mineral water. Then, citric acid (CA) and ethylene glycol (EG), used as polyesterification precursors, were added to the solution (salt:CA:EG molar ratios 1:4:4) and water was slowly evaporated by heating on a hot plate. The highly viscous mixture formed after polyesterification was annealed at 400 °C for 5 hours under air. A dark brown powder was then obtained. Thereafter, various thermal post-treatments were performed at 500 °C under air atmosphere during 10 hours.

The SLS experiments have conducted using a laser system equipped with a IPG Photonics ytterbium fiber laser (YLM-400-AC*Y11) delivering a power up to 400 Watt at a monochromatic wavelength of 1.07 µm, and a galvanometric mirrors scanner (ScanLab - Hurry scan 20).

2.2. Characterization techniques

X-ray diffraction patterns were recorded on a Philips X'Pert MPD apparatus equipped with a copper $K_{\alpha 1}$ anticathode (40 kV, 40 mA). Diffraction patterns were collected from 8 to 80° in 2θ with a 0.017° step scan and a counting time of 5 s.

The morphology of the as-prepared particles was observed thanks to a Leica DMI 3000 M inverted microscope using a Leica SFL 100 diode enabling an excitation at 365 nm and the fluorescence collection recorded with a Leica MC 120 HD camera. Microscope objective N PLAN EPI 10×, NA 0.25 was used. For microstructural analyses, SEM investigations were performed using a TESCAN Vega II SBH microscope or JEOL JSM-6700F. The film thickness was measured by the Dektak 150 Surface Profiler (Veeco), fitted with a stylus which had a radius of 12.5 µm and a resolution of 0.8 µm.

The photoluminescent properties were analysed using a spectrofluorimeter SPEX FL212 equipped with a 450 W Xenon lamp. The excitation spectra were corrected for the variation of the incident flux as well as emission spectra for the transmission of the monochromator and the response of the photomultiplier. This equipment was also used to record diffuse reflectance spectra. In this case, the emission and the excitation monochromator were set in a synchronous mode, in order to collect all the diffuse reflection of the xenon lamp without catching any fluorescence photon. A black reference (B: black toner) and a white reference (W: Magnesia MgO) were scanned in the same conditions and the measurement from the sample (S) was corrected to obtain the desired data (D) following the relation: D = (S-B) / (W-B). The x and y chromatic coordinates were directly determined from the emission spectra.

Finally, the micro-luminescence was carried out with a Labram 800-HR spectrophotometer (Horiba Jobin-Yvon) equipped with an Olympus microscope objective (10x), a CW laser diode excitation at 405 nm (100 mW) and a thermoelectric cooled CCD camera (Synapse Model 354308).

3. Results and discussion

3.1. Powder sample properties

Two thermal sensors were chosen for their ability to mark temperatures variation induced by the laser –matter interaction during the SLS process across the irradiated zone. The choice takes benefit in both cases of the capacity of Mn^{2+} luminescent cation in inorganic oxides to get an emission colour which can drastically vary from red to green while the coordination site of the cations is, irreversibly, modified when a thermal treatment is applied to the Mn-doped oxide compound.

The first material is the manganese doped zinc phosphate phosphors. First the hopeite hydrated form ($Zn_{2.94}Mn_{0.06}(PO_4)_2$,$4H_2O$) is obtained by co-precipitation and then this compound is pre-annealed at 500°C to prepare the anhydrous compound (Mn-doped $Zn_3(PO_4)_2$) in the α-monoclinic form [23, 25-28]. In the α-form as the starting material, the Mn^{2+} ions are located in two non-equivalent distorted tetrahedral sites (Figure 1a). The β and γ phases are the two high-temperature forms. In these forms, the Mn^{2+} ions are located in distorted octahedral and five-fold coordination sites (Figure 1a) [23,27]. Mn^{2+} ions possess d_5 electronic configuration; the main phenomenon of this luminescent dopant corresponds to a $^4T_1 \rightarrow {}^6A_1$ transition, which is strongly dependent on the ligand field and so the coordination number. Hence, the phase transition from the α-form to the γ- or β-form results in a strong modification of the ligand field around the Mn^{2+} ions with an increase in the coordination number. A decrease of the crystal field strength around the Mn^{2+} ions leads to a shift in the Mn^{2+} luminescence emission from green to red [23,29]. Phase transition phenomena from the α-form to the high polymorphs take progressively place for thermal treatments in the temperature range from 700 to 1000°C.

The second material which is going to be used as thermal-history sensor is manganese-doped zinc aluminate spinel. The optical properties of Mn-doped $ZnAl_2O_4$ were shown to depend on the location of Mn^{2+} ions within the spinel network. Spinel structure is a multisite matrix including both

octahedral and tetrahedral sites as potential cationic sites for Mn^{2+} ions [24, 30]. This luminescent ion substituted for Zn^{2+} may occupy octahedral and/or tetrahedral sites depending on synthesis parameters, especially the annealing temperature (as evidenced above). From of Mn-doped $ZnAl_2O_4$ sample prepared at relatively low temperature from Pechini process [31], a drastic change in the emission spectra was observed as temperature increases from 1000 °C to 1400 °C, which also dependent on the Zn/Al molar ratio. This emission property is changing versus the thermal post-treatment by a progressive migration of both manganese and zinc cations into the tetrahedral coordination polyhedral sites. In a previous paper [24], for the 0.5% Mn-doped $ZnAl_{2.2}O_{4+\delta}$ sample, as-prepared in this study, the luminescent properties were already shown to change, for temperature evolution from 800°C to 1400°C, from an emission spectrum with a double contribution in the green range (associated with Mn^{2+} in tetrahedral coordination) and in the red part of the spectrum (associated with Mn^{2+} in octahedral coordination) to an emission spectra with only the occurrence of the green emission band.

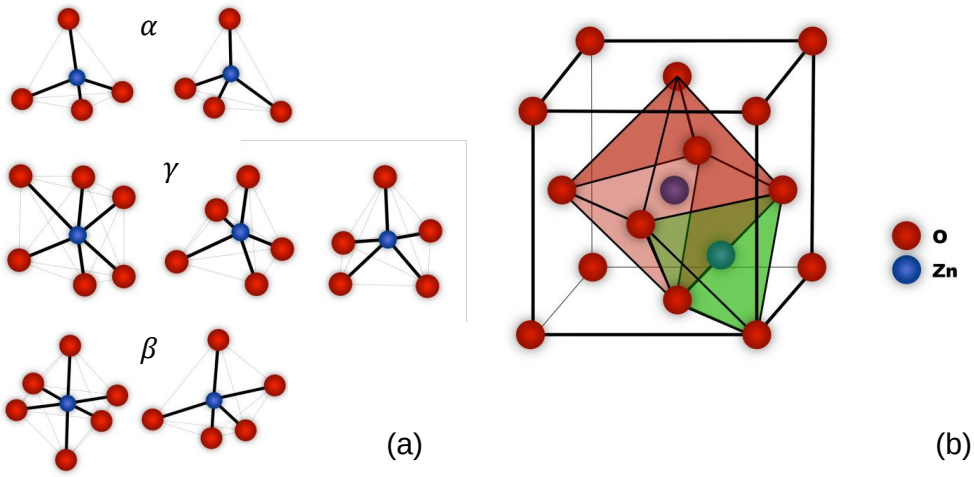

Figure 1. Representation of the various cationic sites (a) in the different α, γ, and β allotropic forms with $Zn_3(PO_4)_2$ composition and (b) in the spinel structure with $ZnAl_2O_4$ composition showing both octahedral (red) and tetrahedral sites (green)

(double column width)

Confirming our previous results with the temperature increase [24], the structural variations were emphasized by X-ray diffraction studies (Figure 2a) for the anhydrous $Zn_{2.94}Mn_{0.06}(PO_4)_2$ compound. The annealing time was fixed to 10 min and followed by an air quenching. When the temperature is increased from 600 to 900°C, the intensities of the diffraction peaks assigned to the γ phase increase whereas the α peak intensities decrease, indicating a phase transition phenomenon. At higher temperatures, between 900°C and 1000°C, an additional phase transition corresponding to the γ→β form is observed. It can be noticed that an annealing treatment at 1100°C followed by a rapid quenching produced the melting of the compound.

With the same post-treatments, for the $Zn_{0.95}Mn_{0.05}Al_{2.2}O_{4+\delta}$ samples, as shown by the X-ray spectra, a pure spinel form is obtained (Figure 2b). The crystallite size, from Debye-Scherrer equation based on diffraction peak width, varies from less than 20 nm for an annealing temperature of 600°C up to 55 nm for thermal treatment at 1400°C. Regarding our previous work [25], the increase of the crystallite size should be associated with a change in the cationic distribution, especially with a decrease of the manganese ions amount located into the octahedral sites while the average particle size is enlarged.

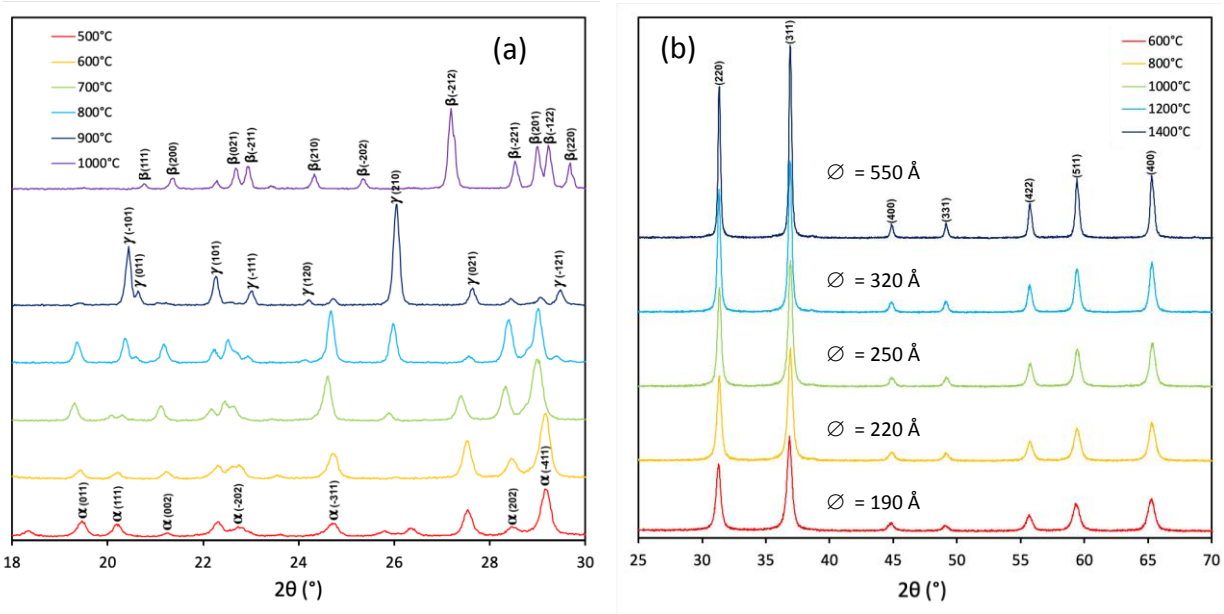

Figure 2. X-ray diffraction patterns of (a) $Zn_{2.94}Mn_{0.06}(PO_4)_2$ and (b) $Zn_{0.95}Mn_{0.05}Al_{2.2}O_{4+\delta}$ obtained by annealing 10 min.at different temperatures and followed by air quenching (∅ means average crystallite size).

(double column width)

The evolution of the luminescence spectral distribution as a function of the annealing temperature for the phosphate compound is plotted in Figure 3a. For an excitation at 405 nm, two contributions of manganese luminescence for an annealing treatment at temperatures lower than 850°C are clearly visible. A first band is centred at approximately 530 nm and a second one is located at 640 nm (*i.e.* lower energy). They correspond respectively to the $^4T_1 \rightarrow {}^6A_1$ transitions of Mn^{2+} in tetrahedral and in octahedral polyhedra. The green emission is then correlated to manganese location in a low coordination site (four-fold coordination site) of the low-temperature form (α-form). The red – orange contribution is issued from Mn^{2+} ions in five- and six-fold coordination sites in the appearing y phase with the annealing treatment temperature increase. For the low annealing temperature range (up to 800°C), we have observed experimentally that the green luminescence intensity increases versus temperature. The increase of the luminescence efficiency is commonly due to the increase of the crystallite size. But, the target here is to sense the temperature not from a change of efficiency but from a change of the chromaticity of the luminescence (the luminescence intensity is difficult to extract in a robust way and to correlate with the thermal history since the luminescence intensity depends on many extrinsic parameters as the powder bed thickness, the spectrometer efficiency, the filters used, the excitation wavelength, *etc.* [32]). By increasing the annealing treatment (T>900°C), the green emission is drastically quenched in favour of the red one, which clearly indicates the disappearance of the α allotropic form of the zinc phosphate phase. The evolution of the emission properties as a function of temperature can be summed up by the plot of the x and y coordinates (of the x,y,z trichromatic color space) (Figure 3b) of the Mn-doped zinc phosphate sample versus the thermal treatment temperature. The chromaticity path following the heat-treatment temperature shows that an accurate characterization of the annealing temperature can be efficiently extracted from the sample emission properties for annealing temperatures varying between 700°C and 1000°C; especially the sample is a very sensitive sensor able to mark a change of temperature between 800 and 850°C, a large optical contrast taking place between the two samples obtained at these temperatures.

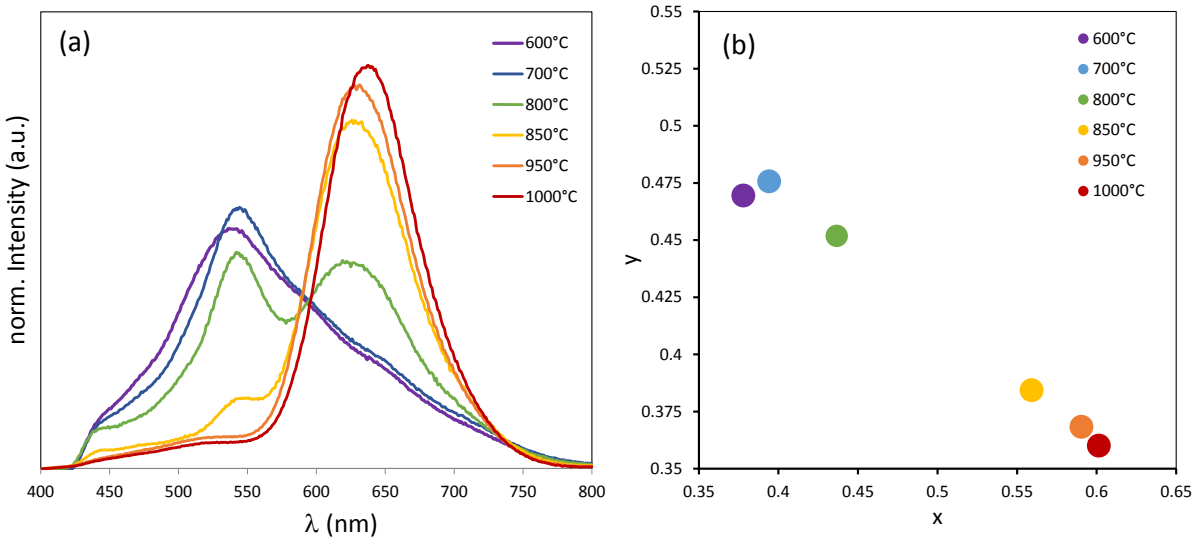

Figure 3. (a) Luminescence spectra and (b) chromatic x and y parameters of the $Zn_{2.94}Mn_{0.06}(PO_4)_2$ sample heated from 600°C to 1000°C during 10 min and then quenched.

(double column width)

The evolution of the luminescence spectral distribution and the X, Y colorimetric parameters as a function of the annealing temperature for the $Zn_{0.95}Mn_{0.05}Al_{2.2}O_{4+\delta}$ spinel powder compound are plotted in Figures 4a and 4b, respectively. As for the previous sample, for an excitation at 405 nm, two contributions of manganese luminescence for an annealing treatment at temperatures lower than 900°C, with a first band centred at approximately 560 nm and a second one located at a lower energy at 700 nm can be observed. Once again, they correspond respectively to the $^4T_1 \rightarrow {}^6A_1$ transitions of Mn^{2+} ions in tetrahedral and octahedral environment, respectively. For treatment temperatures between 600°C and 1000°C, and especially between 800°C and 1000°C, the green contribution intensity increases to the detriment of the red emission intensity. Thus, a reverse chromaticity modification, in regard of the previous zinc phosphate compound, is observed for the spinel sample. Then, for treatment temperatures higher than 1000°C, another phenomenon is detected with a new contribution, constituted by a discrete series of fine peaks in the red region. This series of discrete peaks, based on our previous works devoted to the luminescence of un-doped $ZnAl_2O_4$ compound, is compatible with the spectral signature of a d^3 element. Considering the synthesis route and the composition, these lines should be attributed to Cr^{3+} or Mn^{4+}. We cannot discard the presence of chromium impurities in precursor materials as this element is often detected

due to trace impurities in the aluminium. The lines peaking in the red range are in a good agreement with the E_g-$^4A_{2g}$ R-, N- zero phonon lines of trivalent chromium in the octahedral site of the aluminium ions [30, 33]. The emission spectra also contain satellite lines distributed around the main peak, which can be identified as vibronic (phonon assisted transitions) sideband transitions of Cr^{3+} ions. We can suppose that the Cr^{3+} luminescence is quenched by the structural defects present in smallest crystallites; only a very high annealing temperature treatment reveals the chromium presence. A stabilization of Mn^{4+} is also possible because of the heat-treatment at high temperature performed in air atmosphere. This will also be consistent with the decrease of the green emission between 1000°C and 1200°C. Thus the evolution of the spinel compound's emission properties as a function of temperature can trace the temperature within the 800°C to 1000°C range from the change of the green / red emission band ratio of the Mn^{2+} phosphor. Furthermore, the brutal appearance of the specific luminescence lines associated to the Cr^{3+} impurities and/or Mn^{4+} ions allow the clear indication of a reached temperature of 1200°C at least.

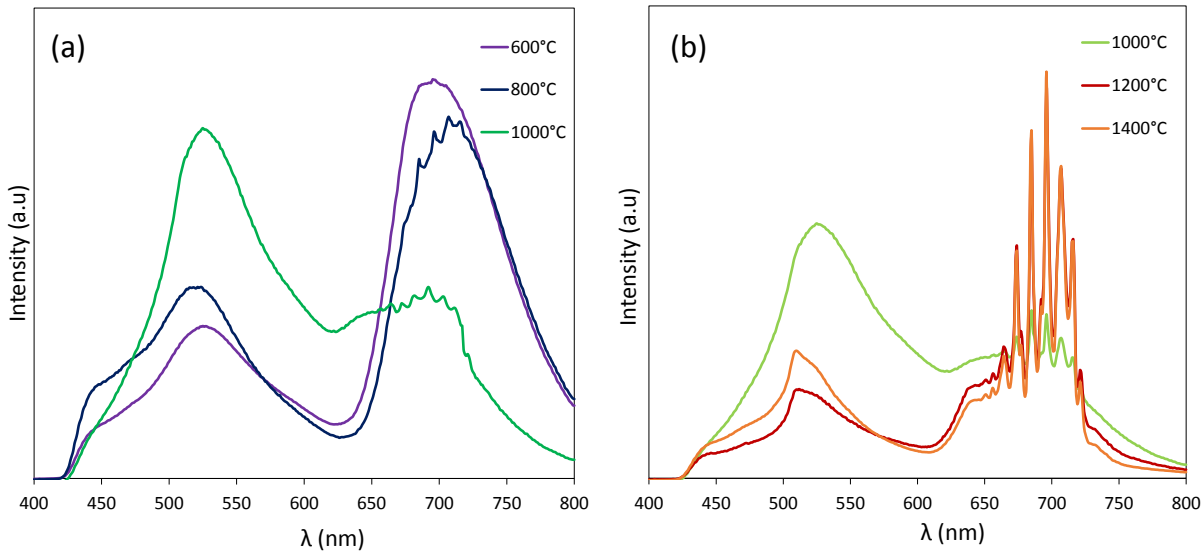

Figure 4. Luminescence spectra of the $Zn_{0.95}Mn_{0.05}Al_{2.2}O_{4+\delta}$ sample heated from 600°C to 1000°C (a) from 1000 °C to 1400 °C during 10 min and then air quenched.

(double column width)

3.2. Film preparation and properties

The two as-prepared thermal sensors are then deposited on silica glass substrates for film preparation using Dr. Blading as film coating process (illustrated in Figure 5a). In a first step, the powder is dispersed in ethanol (30-35 wt%) and ultra-sonication is used to improve the dispersion quality. A viscous suspension thanks to the high powder concentration that can be coated in a facile way with the blade apparatus is so obtained. Thickness was adjusted thanks to razor blade to about 40 μm – 50 μm as shown by the film profile obtained by interferential profilometry taking 0 height at the glass substrate surface (Figure 5f), *i.e.* a thickness which can be considered inferior to the penetration depth of the laser ensuring a quite homogeneous energy along the cross section.

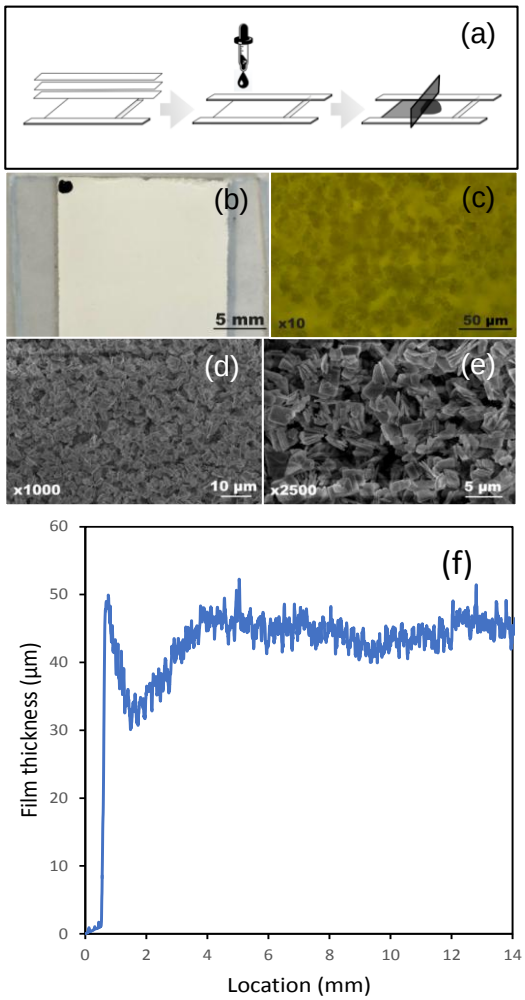

Figure 5. (a) Schematic drawing of the "Dr. Blade deposit process to obtain the ceramic film. Illustration of the microstructure obtained for the Mn^{2+}-doped $Zn(PO_4)_2$ film. (b) & (c) macroscopic view and optical microscope images and (d) & (e) SEM images of the film, (f) Thickness of the fiml estimated form the optical profilometer. ***(single column width)***

After the coating, the films are dried in an oven at 100°C for 2 hours, and a pre-annealing treatment at 500°C during 10 min was performed. The as-prepared films, for both the phosphate and the spinel samples, are white, with homogeneous surface, as illustrated by the optical microscope pictures for the phosphate sample in Figure 5b, 5c. SEM micrographs reveal that the starting films are highly porous with porosity about 50%. Both can be described as a powder bed constituted as a pack of micron-size aggregates. The two SEM pictures with different magnification reported in Figures 5d and 5e illustrates the high porosity rate. However thanks to the annealing pre-treatment, the films are easily handled; however the films can be removed by fingers scratches.

SLS process was firstly applied to the Mn-doped Zn_3PO_4 film, varying the power of the laser and/or the laser scanning speed. Thanks to the quick SLS processing to write laser tracks, different sets of parameters have been tested. The aim is not to optimize here the SLS parameters but to detect if post mortem, the material luminescence modification could indicate the reached temperature. Hereafter, we have chosen to illustrate our work on a Mn^{2+}-doped $Zn(PO_4)_2$ film after the application of the laser as horizontal lines with various laser scanning speeds and laser powers, with high energy for the laser (low speed and/or high power) (Figure 6). Most of the lines reflect a too high deposited energy and the film is clearly melted because the lines appear with glassy and transparent aspect under white light. This transparent aspect can be evidenced by photographs of the film deposited (or coated) on its glass substrate on a black support as illustrated in Figure 6a. The access to the melting point is evidenced by the presence of air bubbles embedded in the glassy lines as shown in the insert of the Figure 6b showing the laser strikes obtained for the largest dose deposition. Surprisingly, a luminescence halo with high intensity is detected around these lines. This is not a green to red chromaticity evolution with the proximity of the glassy part, but, on the contrary, a homogeneous bright greenish chromaticity. Hence, the red emission corresponding here to the presence of the high temperature forms seems by-passed. May some film parts have transited through the high temperature form, but in any case, the high temperature form is nowhere stabilized. Indeed, a brutal modification from a low green luminescence attesting the presence of low

temperature forms far from the lased lines (at least with Mn^{2+} remaining inside a tetrahedral coordination) to a halo around the glassy lines with green luminescence is observed. Because of the high intensity of the green-emissive halo around the glassy lines, it is difficult to observe the luminescence of the glassy parts, even using confocal microscope. The green luminescence halo is, by the way, fully compatible with the beginning of ceramic to glass transformation, Mn^{2+} in low concentration in glass systems showing green luminescence [34].

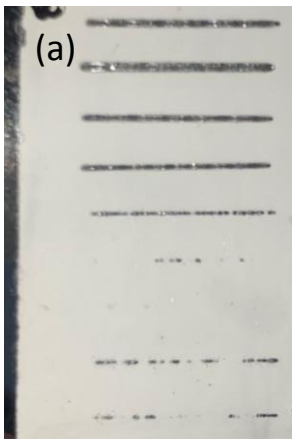

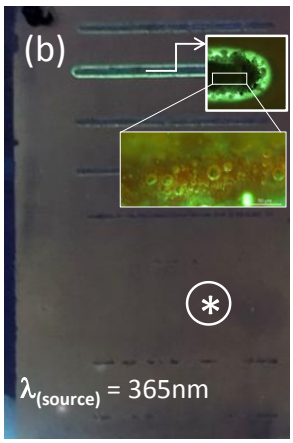

Scanning speed (mm.s^{-1})	Power (W)
35	50
18	34
35	34
35	30
35	20
29	17
29	16
41	18
15	29

Figure 6 (a) Photograph under white light source of Mn^{2+}-doped $Zn_3(PO_4)_2$ film on a black support after the application of the laser as horizontal lines with various laser scanning speeds and laser powers, (b) Photograph under UV-light monochromatic source of the same Mn^{2+}-doped $Zn(PO_4)_2$ film (the inserted photographs are taken with the confocal microscope (λ = 405 nm).

(double column width)

The next experiments are focused on the very small defects observed for the lowest dose deposition of the previous Figure 6b (punctual defects marked with a star). Concentrating our attention on those punctual defects, few balls formed under the laser excitation are shown by SEM (Figure 7a). Accurate analyses of the variation of the luminescence variation of the sample film around the formed balls are performed using confocal microscopy (Figure 7 b). Emission spectra are recorded on the micrometric analysis zones which are marked from 1 to 7 (Figure 8a), X, Y color parameters are reported in Figure 8b.

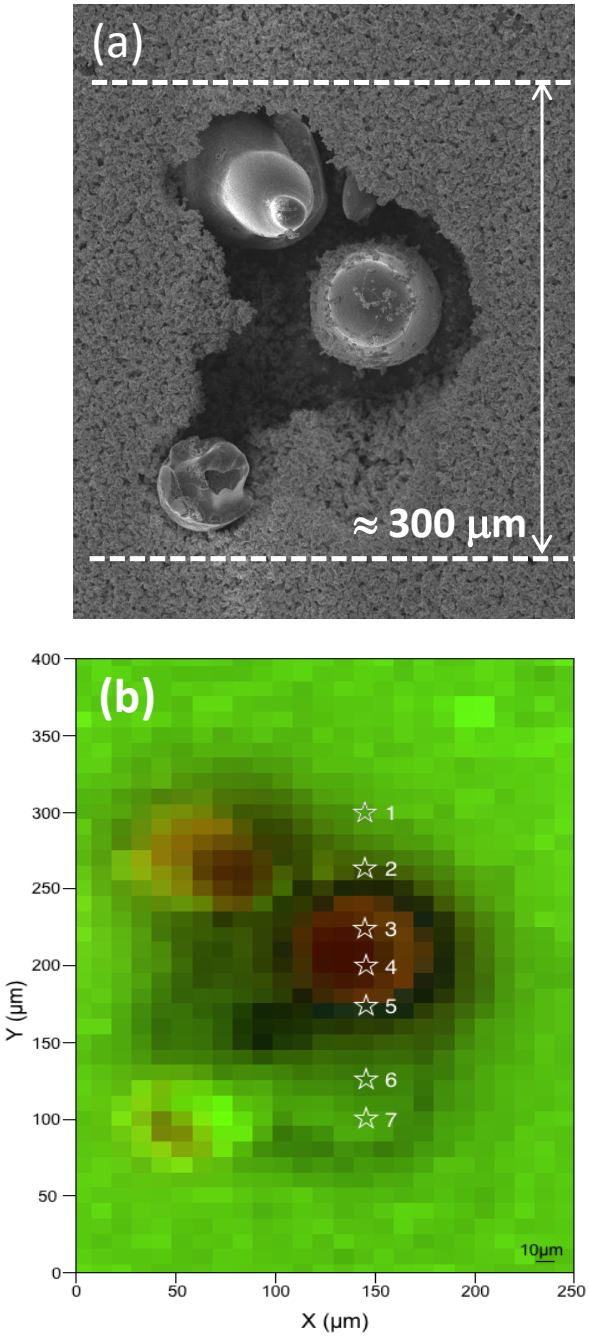

Figure 7. (a) SEM image of the $Zn_{2.94}Mn_{0.06}(PO_4)_2$ film with "ball effect" on the lased area and (b) corresponding luminescence cartography from confocal microscopy **(single column width)**

As it can be seen in Figure 7a, the laser irradiation follows a line of about 300 µm width. Apart from the formation of few balls, as punctual defects, the laser seems to have no sintering activity, based on the morphology of the particles constituting the powder film. Using the confocal microscope, the analysed points are along a straight line which crosses the largest ball formed by the

laser interaction. The luminescence spectrum suddenly changes in the ball location from green to red. Outside this region, the film even after the laser irradiation still exhibits a main green emission band (about 525 nm) coupled with as low contribution, a minor intensity red band (around 600 nm, Figure 8a). Hence, while the laser is applied with this intermediate scanning speed and low power value (29 $mm.s^{-1}$, 16 W), the transferred energy is not sufficient to produce the phase transition from the Mn^{2+}-doped $Zn_3(PO_4)_2$ low temperature form (within tetrahedral sites) to the high temperature form (within octahedral sites). Thus, basing on the emission powder properties reported in Figure 3, the laser allows *a priori,* the maximal temperature level is remaining below 800°C for the points 1,2,6 and 7 whereas temperature seems to be between 800°C and 900°C for the points 3 to 5 (Figure 3).

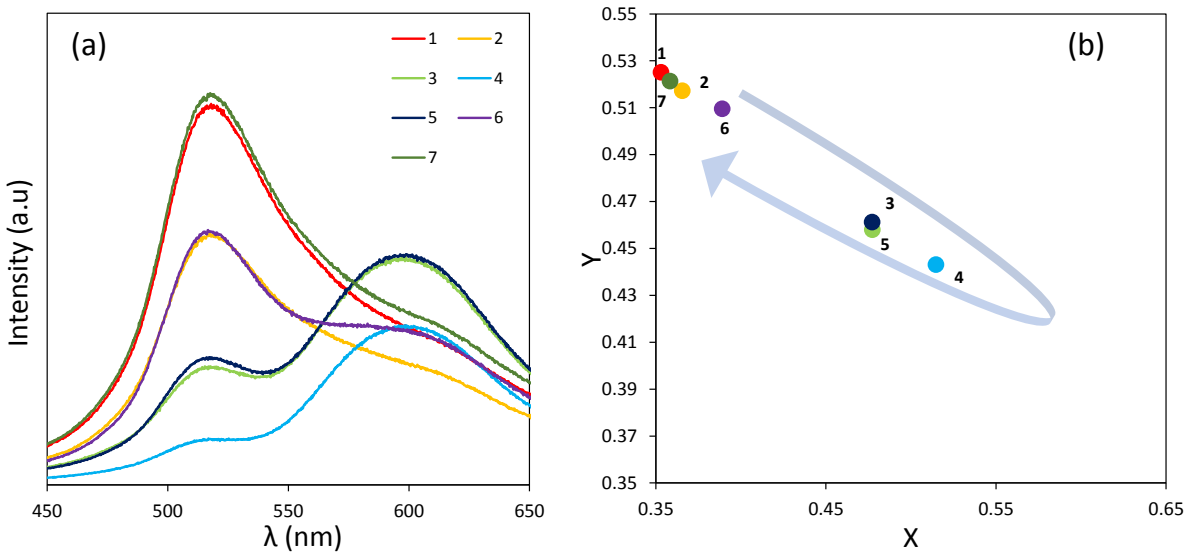

Figure 8. (a) Luminescence spectra of the $Zn_{2.94}Mn_{0.06}(PO_4)_2$ film recorded on the 7 analysis points and (b) the corresponding chromatic x and y parameters (plot in same scale than for Figure 3b.)

(double column width)

Nonetheless, the formed ball offers an emission spectrum showing a red luminescence band as main band, coupled with, as minor band, the green emission one. According to the perfect spherical shape of the ball, one can assume that this zone well corresponds to a punctual hot spot with a local heating close to the vicinity of the melting point. Additionally, the structural feature of the ball is not similar to the rest part of the film, with Mn^{2+} ions located into octahedral sites, as in the zinc phosphate high temperature form. As conclusion on the possibility of using the Mn-doped

zinc phosphate, severe restrictions need to be expressed. Although the change from the low to the high temperature form should occur significantly below the phase transition occurs on the range from 700 to 900°C (the melting point takes place between 1000 and 1100°C). One can suspect that the working temperature range is here too narrow or with too low kinetic in regard of the absorption at the laser wavelength too high and the temperature diffusion too slow. The differences observed between the set of powder samples, annealed 10 min in a furnace, and the film submitted to the laser irradiations, take place without any doubt on the very different kinetic conditions between these two sample sets. With a speed of 29 $mm.s^{-1}$ and laser track of 1.5 cm length, the irradiation time to plot a full line is about half a second. The powder absorbing do not diffuse the temperature fast enough to avoid the melting. Apparently, the change of structural form, *i.e.* the phase transition between the low and high crystallographic forms which is not detected, has no time to efficiently occur before the sample melting. A sensor based on such a phosphate structural phase transition seems not well adapted to extract temperature cartographies in a fast heating process.

SLS process was secondly operated on the Mn-doped $ZnAl_2O_4$ film, with the same procedure (varying again the power of the laser and/or the laser scanning speed). Briefly and focusing straight on the best results, one can concentrate on a lased tracks using a scanning speed: laser power parameters: 50 $mm.s^{-1}$ and 72 W. It can be noted that the spinel absorption at 1 µm is lower than the phosphate phase absorption. Significantly higher laser power must be used for heating. Macroscopically and microscopically, no clear effect that the melting or an advanced sintering is observed on the irradiated area. Accurate analyses of the variation of the luminescence variation of the sample film across the lased line, extracted from optical microscope (top picture) and from confocal microscopy (bottom picture), are shown in Figure 9 (8 analysis points). Clearly, on the picture depicted from the confocal microscopy, the centre of the line is associated with a greenish luminescence whereas the un-lased part of the film is associated with reddish luminescence.

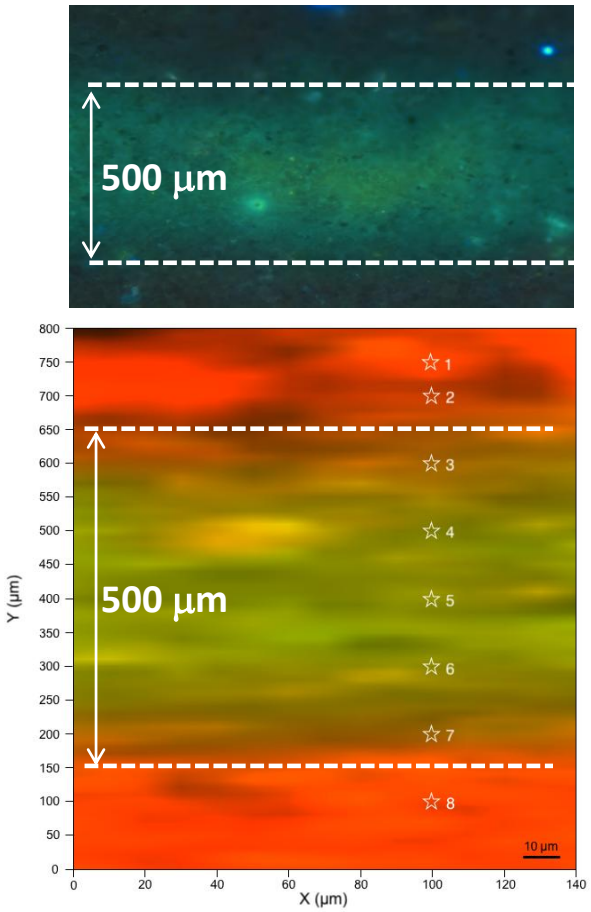

Figure 9. (top) Optical microscope image on the $Zn_{0.95}Mn_{0.05}Al_{2.2}O_{4+\delta}$ film (focus on a lased area) and (bottom) corresponding luminescence cartography from confocal microscopy

(single column width)

The emission spectra corresponding to the eight analysis points are reported in Figure 10a; corresponding x, y chromatic parameters calculated from each spectrum are plotted in Figure 10b. A clear gradual evolution from the outside to the centre of the lased line can be observed. A progressive switch from emission spectra dominated by the red range band (centred at 700 nm) to emission spectra dominated by the green range band (at 520 nm) is evidenced. In regard of the powder reference samples annealed 10 min, the temperature gained during the irradiation progressively increases up to 1000°C from far to the centre of the area impacted by the laser. Kinetic aspects are herein, on the contrary to what it has been noted for the phase transition of the zinc phosphate compounds, not a drastic limitation of the analysis. This aspect may be related to the lower absorption of the aluminate as compared to the phosphate phase which favour diffuse

reflectance and more homogeneous absorption and heating and/or the kinetic of the mechanism at the origin of the thermochromism in these two phases. Indeed, the change of the luminescence originates from the cationic reorganization in the spinel multisite matrix (with both octahedral and tetrahedral sites). No energy barrier has to be crossed, and the cation distribution has to be directly linked to the thermal history, whatever the duration of the heating time.

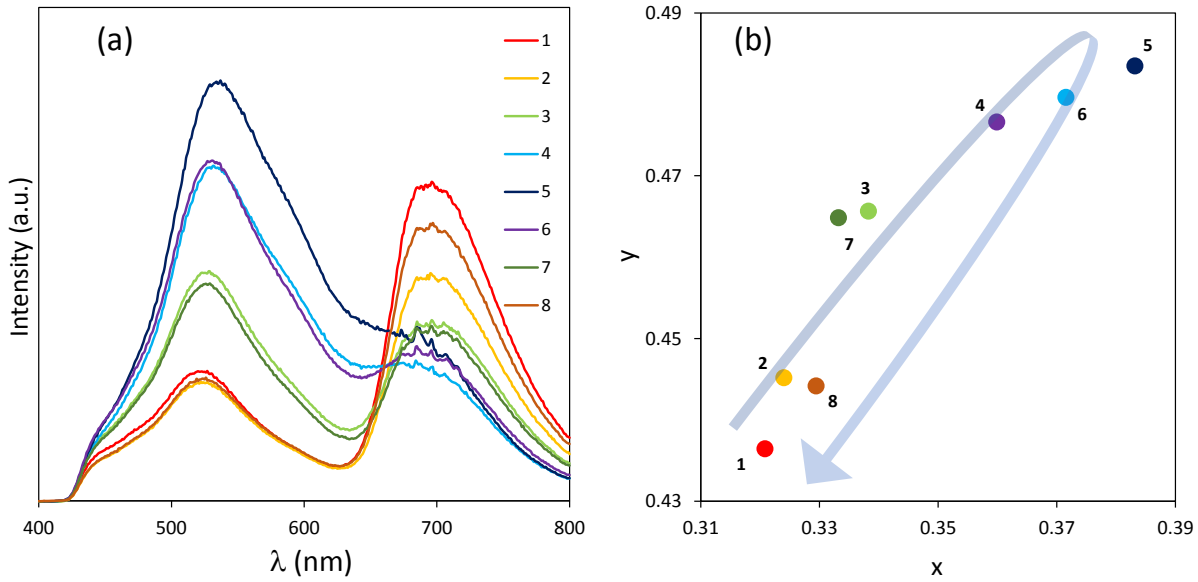

Figure 10. (a) Luminescence spectra of $Zn_{0.95}Mn_{0.05}Al_{2.2}O_{4+\delta}$ film recorded on the 8 analysis points and (b) the corresponding chromatic x and y parameters.

(double column width)

A high energy couple of parameters (laser scanning speed and laser power: 75 mm.s^{-1} and 96 W, respectively) has also been tested on the spinel film. Increasing the laser energy, as previously observed on the zinc phosphate film, the film starts to be deteriorated, showing scratched zones (Figure 11, top side). Photographs made by optical microscopy under UV-light excitation show the lased line exhibits very intense luminescence, especially near the scratched defects. Emission spectra on points near the scratched defects were recorded using confocal microscopy in order to check that the scratched areas are well corresponding to hot spots, as observed in the previous study. The luminescence properties of three analysed micrometric points were recorded for discussion: the first

one far away from the hot spot, the third one on the hot spot, and the second one in intermediate location (Figure 11, bottom).

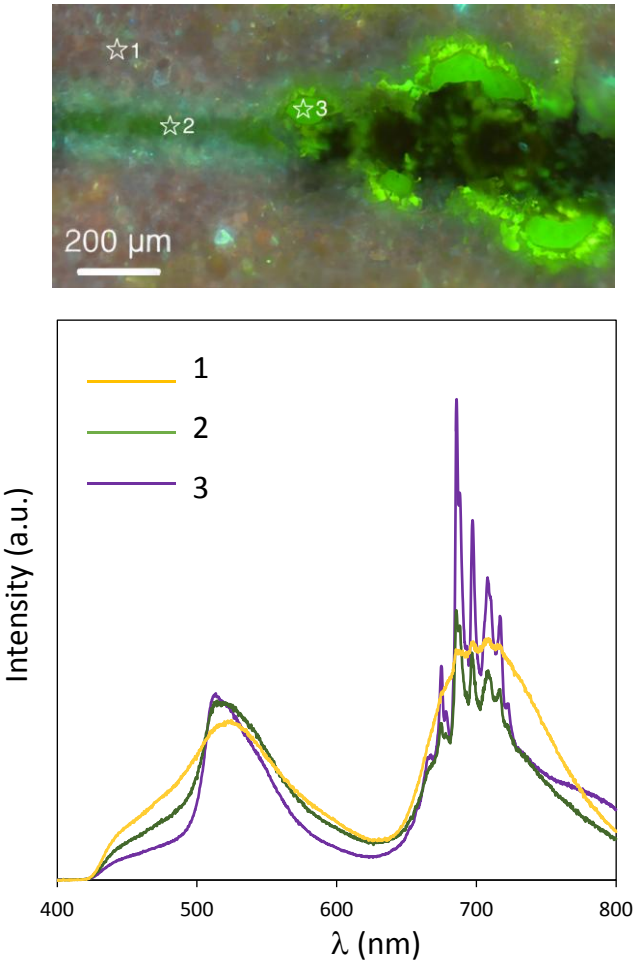

Figure 11. (top) Optical microscope image on the $Zn_{0.95}Mn_{0.05}Al_{2.2}O_4$ film (focus on a lased path line) and (bottom) the corresponding luminescence spectra of recorded on the three analysis points.

(single column width)

From the emission spectra (Figure 11, bottom), it can be concluded that the scratched defects are well associated with hot spots. Indeed, these areas get a strong emission linked to the Cr^{3+} impurities or Mn^{4+} ions, which was shown to be revealed only by very high temperature treatments over 1200°C (Figure 4b). Manganese-doped spinel material as temperature sensor gets not only the capacity to mark temperature transition from 800°C to 1000°C from the red to green luminescence variation but it is also adequate, from the sudden appearance of the discrete red

emission lines, to mark the raise of temperatures over 1200°C during thermal history, thanks to the presence of the series of discrete and fine peaks in the red region.

Conclusion

In this article, based on our previous studies, two home-prepared compounds: Mn^{2+}-doped $Zn_3(PO_4)_2$ and Mn^{2+}-doped $ZnAl_{2-2}O_{4+\delta}$ were used as thermal sensors, thanks to their thermochromoluminescence properties, as SLS process probe. Our work may be particularly useful for printing of mixed materials such as in situ alloying and composites rather than a single material, using then, for illustration, the spinel compound mixed as minor rate to record the thermal history of an alloy as main compound (composite matrix). Composite materials, in this way, have been recently shaped from SLM additive manufacturing [35, 36]. The target of the study was to be able to extract from the emission spectra of the materials a real idea of the temperatures that are reached during the laser – matter interaction. In a first part, the luminescent chromaticity of both the as-prepared compounds versus the annealing temperature (for 10 min. annealing treatments) was plotted, as abacus curves. The changes of the emission spectra were *a priori* well-adapted to mark temperature in the range 600-1200°C, for a temperature gradient of 500°C versus no more than 100 microns about. Chen Bo et al. studies [37] on SLM have shown that it is possible to estimate on alloys the melt pool dimension (about 0.36 mm × 0.21 mm) based on appropriate thermal imager setting (thermography), but with difficulties to extract the true temperatures. This comparison with alternative processes in order to record thermal history shows that both thermal resolution and spatial resolution proposed herein are competitive. For the Mn-doped zinc phosphate, large differences were observed between the abacus curve from the annealed powders and the change of the optical properties observed on doctor bladed film submitted to the laser irradiations. This can be interpreted as a consequence of a local absorption which is too high in the phosphate compound and/or the different kinetic condition between these two studied compounds; avoiding the phase transition at the origin of the thermochromoluminescence in the case of the “ultra-rapid’ heating

using laser irradiation. On the contrary, for the spinel compound, the change of the luminescence originates from the cationic reorganization in the spinel multisite matrix and the comparison between the abacus curves obtained on annealed powders and laser-irradiated films have shown that for both cases, the emission spectra are directly linked in a same way to the maximal temperature gained during the thermal history, whatever the duration of the heating time. This material can so be used as thermal sensor for SLS process.

References

[1] W.E. Frazier, Metal additive manufacturing: a review, J. Mater. Eng. Perform. 23 (2014) 1917–1928, http://dx.doi.org/10.1007/s11665-014-0958

[2] L. Ferrage, G. Bertrand, P. Lenormand, Dense yttria-stabilized zirconia obtained by direct selective laser sintering, Additive Manufacturing 21 (2018) 472-478, https://doi.org/10.1016/j.addma.2018.02.005

[3] L. Ferrage, G. Bertrand, P. Lenormand, D. Grossin, B. Ben-Nissan, A review of the additive manufacturing (3DP) of bioceramics: alumina, zirconia (PSZ) and hydroxyapatite, J. Aust. Ceram. Soc. 53 (2017) 11–20, http://dx.doi.org/10.1007/s41779-016-0003-9

[4] I. Yadroitsev, P. Bertrand, I. Smurov, Parametric analysis of the selective laser melting process, Appl. Surf. Sci. 253 (2007) 8064–8069, http://dx.doi.org/10.1016/j.apsusc.2007.02.088

[5] S.F.S. Shirazi, S. Gharehkhani, M. Mehrali, H. Yarmand, H.S.C. Metselaar, N.A. Kadri, N.A.A. Osman, A review on powder-based additive manufacturing for tissue engineering: selective laser sintering and inkjet 3D printing, Sci. Technol. Adv. Mater. 16 (2015) 033502, http://dx.doi.org/10.1088/1468-6996/16/3/033502

[6] J.W. Stansbury, M.J. Idacavage, 3D printing with polymers: challenges among expanding options and opportunities, Dent. Mater. 32 (2016) 54–64, http://dx.doi.org/10.1016/j.dental.2015.09.018

[7] A. Simchi, Direct laser sintering of metal powders: Mechanism, kinetics and microstructural features, Mater. Sci. Eng. A 428 (2003) 148-158, http://dx.doi:10.1016/j.msea.2006.04.117

[8] H.C.H. Ho, W.L. Cheung, I. Gibson, Effects of graphite powder on the laser sintering behaviour of polycarbonate, Rapid Prototyp. J. 8 (2002) 233–242, http://dx.doi.org/10.1108/13552540210441148

[9] L. Hao, S. Dadbakhsh, O. Seaman, M. Felstead, Selective laser melting of a stainless steel and hydroxyapatite composite for load-bearing implant development, J. Mater. Process Tech. 209 (2009) 5793–5801. https://doi.org/10.1016/j.jmatprotec.2009.06.012

[10] J. P. Kruth, L. Froyen, J. Van Vaerenbergh, P. Mercelis, M. Rombouts, B. Lauwers, Selective laser melting of iron-based powder, J. Mater. Process. Technol. 149 (2004) 616-622, http://dx.doi:10.1016/j.jmatprotec.2003.11.051

[11] Z. Chen et al., 3D printing of ceramics: A review, J. Eur. Ceram. Soc. 39(2019) 661-687, http://dx.doi:10.1016/j.jeurceramsoc.2018.11.013

[12] J.P. Kruth, P. Mercelis, J. Van Vaerenbergh, L. Froyen, et M. Rombouts, Binding mechanisms in selective laser sintering and selective laser melting, Rapid Prototyp. J. 11 (2005) 26-36, http://dx.doi:10.1108/13552540510573365

[13] H.-H. Tang, M.-L. Chiu, H.-C. Yen, Slurry-based selective laser sintering of polymer-coated ceramic powders to fabricate high strength alumina parts, J. Eur. Ceram. Soc. 31 (2011) 1383–1388, https://doi.org/10.1016/j.jeurceramsoc.2011.02.020

[14] T. Friedel, N. Travitzky, F. Niebling, M. Scheffler, P. Greil, Fabrication of polymer derived ceramic parts by selective laser curing, J. Eur. Ceram. Soc. 25 (2005) 193–197, https://doi.org10.1016/j.jeurceramsoc.2004.07.017

[15] K. Tan, C. Chua, K. Leong, C. Cheah, P. Cheang, M.A. Bakar, S. Cha, Scaffold development using selective laser sintering of polyetheretherketone–hydroxyapatite biocomposite blends, Biomater. 24 (2003) 3115–3123, https://doi.10.1016/S0142-9612(03)00131-5

[16] C. Gao, B. Yang, H. Hu, J. Liu, C. Shuai, S. Peng, Enhanced sintering ability of biphasic calcium phosphate by polymers used for bone scaffold fabrication, Mater. Sci. Eng. C 33 (2013) 3802–3810, https://doi.10.1016/j.msec.2013.05.017

[17] E. Juste, F. Petit, V. Lardot, F. Cambier, Shaping of ceramic parts by selective laser melting of powder bed, J. Mater. Res. 29 (2014) 2086-2094, https://dx.doi:10.1557/jmr.2014.127

[18] K. G. Prashanth, S. Scudino, T. Maity, J. Das, J. Eckert, Is the energy density a reliable parameter for materials synthesis by selective laser melting?, Mater. Res. Lett. 5 (2017) 386-390, http://dx.doi:10.1080/21663831.2017.1299808

[19] K. Shahzad, J. Deckers, Z. Zhang, J.-P. Kruth, J. Vleugels, Additive manufacturing of zirconia parts by indirect selective laser sintering, J. Eur. Ceram. Soc. 34 (2014) 87–95, https://dx.doi.org/10.1016/j.jeurceramsoc.2013.07.023

[20] S. Das, Physical Aspects of Process Control in Selective Laser Sintering of Metals, Adv. Eng. Mater. 5 (2003) 701-711, https://dx.doi:10.1002/adem.200310099

[21] L. Hao, M.M. Savalani, Y. Zhang, K.E. Tanner, R.A. Harris, Selective laser sintering of hydroxyapatite reinforced polyethylene composites for bioactive implants and tissue scaffold development, Proc. I Mech E Part H, J. Eng. Med. 220 (2006) 521–531, https://dx.doi:10.1243/09544119JEIM67

[22] N. K. Tolochko et al., Balling processes during selective laser treatment of powders, Rapid Prototyp. J. 10 (2004) 78-87, https://dx.doi:10.1108/13552540410526953

[23] G. Salek, A. Demourgues, A. Garcia, V. Jubera, M. Gaudon, Mn^{2+} doped $Zn_3(PO_4)_2$ phosphors: irreversible thermochromic materials useful as thermal sensors, Opt. Mater. 47 (2015) 323-327, https://dx.doi:10.1016/j.optmat.2015.05.049

[24] L. Cornu, M. Duttine, M. Gaudon, V. Jubera, Luminescence switch of Mn-Doped $ZnAl_2O_4$ powder with temperature, J. Mater. Chem. C 1 (2013) 5419-5428, https://dx.doi:10.1039/c3tc30964a

[25] L. Robertson, M. Gaudon, S. Pechev, a. Demourgues, Structural transformation and thermochromic behavior of Co^{2+}-doped $Zn_3(PO_4)_2{\cdot}4H_2O$ hopeites, J. Mater. Chem. 22 (2012) 3585, https://doi.org/10.1039/C2JM14759A

[26] O.Pawlig, R.Trettin, Synthesis and characterization of α-hopeite, $Zn_3(PO_4)_2{\cdot}4H_2O$, Materials Research Bulletin, 34 (1999) 1959-1966, https://doi.org/10.1016/S0025-5408(99)00206-8

[27] J.S. Stephens, C. Calvo, Crystal structure of β-$Zn_3(PO_4)_2$, Can. J. Chem. 45 (1967). https://doi.org/10.1139/v67-376

[28] J. Wang, S. Wang, Q. Su, Synthesis, photoluminescence and thermostimulated-luminescence properties of novel red long-lasting phosphorescent materials beta-$Zn_3(PO_4)_2$:Mn^{2+},M^{3+} (M ~ Al and Ga), J. Mater. Chem. 3 (2004) 2569–2574. https://doi.org/10.1039/B401685H

[29] A.L. Smith, Luminescence of Three Forms of Zinc Orthophosphate:Mn, J. Electrochem. Soc. 98 (1951) 363. https://iopscience.iop.org/article/10.1149/1.2778220/meta

[30] L. Cornu, M. Gaudon, and V. Jubera, $ZnAl_2O_4$ as a potential sensor: variation of luminescence with thermal history, J. Mater. Chem. C 1 (2013) 5419. https://doi.org/10.1039/C3TC30964A

[31] M.P. Pechini, U.S. Patent No. 3231328, Jan., 1966.

[32] A. Rabhiou, J. Feist, A. Kempf, S. Skinner, A. Heyes, Phosphorescent thermal history sensors, Sensors and Actuators A 169 (2011) 18-26. https://doi.org/10.1016/j.sna.2011.04.022

[33] V. Mikenda, A. Preisinger, N-lines in the luminescence spectra of Cr^{3+}-doped spinels (I) indentification of N-lines, J. Lumin. 26 (1981) 53-66. https://doi.org/10.1016/0022-2313(81)90169-1

[34] H. Félix-Quintero, I. Camarillo-Garcìa, J. Hernández-Alcántara, E. Camarillo-García, A. Cordero-Borboa, C. Flores-Jiménez, M. García-Hipólito, F. Ramos-Brito, D. Acosta-Najarro, H. Murrieta-Sánchez, RGB emission of Mn^{2+} doped zinc phosphate glass, J. Non-Crystalline Sol. 466–467 (2017) 58–63. https://doi.org/10.1016/j.jnoncrysol.2017.04.002

[35] R. Martinez, I. Todd, K. Mumtaz, In situ alloying of elemental Al-Cu12 feedstock using selective laser melting, Virtual and Physical Prototyping, 14 (2019) 242-252. https://doi.org/10.1080/17452759.2019.1584402

[36] W.H. Yu, S.L. Sing, C.K. Chua, C.N. Kuo, X.L. Tian, Particle-reinforced metal matrix nanocomposites fabricated by selective laser melting: A state of the art review. Progress in Materials Science 104 (2019): 330-379. https://doi.org/10.1016/j.pmatsci.2019.04.006

[37] B. Cheng, J. Lydon, K. Cooper, V. Cole, P. Northrop, K. Chou, Infrared thermal imaging for melt pool analysis in SLM: a feasibility investigation, Journal Virtual and Physical Prototyping. 13 (2018) 8-13. https://doi.org/10.1080/17452759.2017.1392685